RSC Advances

PAPER

Cite this: *RSC Adv.*, 2020, **10**, 16266

Ruthenium carboranyl complexes with 2,2′-bipyridine derivatives for potential bimodal therapy application†

Ricardo G. Teixeira,[a] Fernanda Marques,[b] M. Paula Robalo,[cd] Xavier Fontrodona,[e] M. Helena Garcia,[a] Simonetta Geninatti Crich,[f] Clara Viñas *[g] and Andreia Valente *[a]

Ruthenium complexes of carboranyl ligands offer the possibility of dual action (chemo + radiotherapy) that might result in significant clinical benefits. In that frame, we describe herein the development of ruthenium–carboranyl complexes bearing bipyridyl derivatives with the general formula [3-CO-3,3-{κ^2-4,4′-R_2-2,2′-bipy}-*closo*-3,1,2-$RuC_2B_9H_{11}$] (R = CH_3, **RuCB1** or R = CH_2OH, **RuCB2**). Both compounds crystallized in the monoclinic system, showing the expected three-legged piano stool structure. The ruthenacarboranes are stable in cell culture media and were tested against two cell lines that have shown favorable clinical responses with BNCT, namely melanoma (A375) and glioblastoma (U87). **RuCB1** shows no cytotoxic activity up to 100 μM while **RuCB2** showed moderate activity for both cell lines. Cell distribution assays showed that **RuCB2** presents high boron internalization that is proportional to the concentration used indicating that **RuCB2** presents features to be further studied as a potential anticancer bimodal agent (chemo + radiotherapy).

Received 17th February 2020
Accepted 6th April 2020

DOI: 10.1039/d0ra01522a

rsc.li/rsc-advances

Introduction

Cancer is the second leading cause of death worldwide. Most of the FDA approved anticancer drugs are purely organic molecules, which may include nitrogen, oxygen, and halogens besides carbon and hydrogen, all of them right-hand neighbors of carbon. The successful introduction of cisplatin as an anticancer drug opened the possibility to investigate the potential applications of metal-based compounds in medicine. Many organometallic complexes of Fe(II), Rh(III), Ir(III), Ru(II) and Os(II) have been shown to present modes of action different to cisplatin and related platinum drugs, for which DNA is the main target.[1] Although ruthenium-based organometallic compounds have emerged as promising anticancer drugs due to their unique and versatile biochemical properties only a few of them have been reported comprehensively.[2]

Boron is located on the left side of the carbon in the Periodic Table and both are elements that have the property to build molecules of unlimited size by covalent self-bonding. Essentially, the twelve-vertex $C_2B_{10}H_{12}$ carborane, *ortho*-, *meta*- or *para*-isomers, rank among the most chemical and biological stable molecular compounds known, which display many particular characteristics that do not find a parallel in their organic counterparts.[3] These species have two moderately acidic C–H vertices that are easily deprotonated with strong bases and functionalized using electrophiles.[4] On the other hand, the anionic *nido*-carborane ($[C_2B_9H_{12}]^-$ and $[C_2B_9H_{11}]^{2-}$) derivatives result from the known as "partial deboronation process", which takes place by the attack of a nucleophile[5–13] to the corresponding *closo*-$C_2B_{10}H_{12}$ cluster resulting in the loss of a B vertex. Metallacarboranes, neutral half-sandwich [$M(C_2B_9H_{11})$LL′L″] (L, L′, L″ being anionic and/or neutral ligands) and the anionic sandwich metallabisdicarbollides $[M(C_2B_9H_{11})_2]^-$, are derivatives of boron hydrides that contain carbon and metal atoms into the fragment.[3] A large number of metals have been

[a]*Centro de Química Estrutural, Departamento de Química e Bioquímica, Faculdade de Ciências, Universidade de Lisboa, Campo Grande, 1749-016 Lisboa, Portugal. E-mail: amvalente@fc.ul.pt*

[b]*Centro de Ciências e Tecnologias Nucleares, Instituto Superior Técnico, Universidade de Lisboa, Estrada Nacional 10, 2695-006 Bobadela LRS, Portugal*

[c]*Área Departamental de Engenharia Química, Instituto Superior de Engenharia de Lisboa, Instituto Politécnico de Lisboa, Rua Conselheiro Emídio Navarro, 1, 1959-007 Lisboa, Portugal*

[d]*Centro de Química Estrutural, Complexo I, Instituto Superior Técnico, Universidade de Lisboa, Av. Rovisco Pais, 1049-001 Lisboa, Portugal*

[e]*Departament de Química and Serveis Tècnics de Recerca, Universitat de Girona, Campus de Montilivi, 17071 Girona, Spain*

[f]*Dipartimento di Biotecnologie Molecolari e Scienze per la Salute, Università di Torino, via Nizza 52, 10126 Torino, Italy*

[g]*Institut de Ciència de Materials de Barcelona (ICMAB-CSIC), Campus U.A.B., 08193 Bellaterra, Spain. E-mail: clara@icmab.es*

† Electronic supplementary information (ESI) available: Spectroscopic data for **RuCB1** and **RuCB2** (NMR, FTIR and UV-Vis); crystallographic data and structural refinement details for X-ray data for **RuCB1** and **RuCB2**; stability curves; *in vitro* uptake experiments on A375 cells. CCDC 1980631 and 1980632. For ESI and crystallographic data in CIF or other electronic format see DOI: 10.1039/d0ra01522a

incorporated as cluster vertices in metallacarboranes, keeping the chemical and self-assembly properties of the *closo* carboranes clusters and incorporating the redox properties of the metal.[3]

Boron neutron capture therapy (BNCT) is a non-invasive binary cancer treatment modality that is based on the selective accumulation of a ^{10}B-containing agent at the tumor site followed by irradiation with low-energy neutrons producing high-linear energy transfer (LET) alpha particles ($^{4}He^{2+}$) and recoiling lithium ions ($^{7}Li^{3+}$).[14] These high-energy particles have a short path length (5–9 μm) that is approximately the diameter of a cell. Thus, their action is limited to the cells containing the boron agent, which decreases the damage to normal tissues. However, the success of this therapy is highly dependent on the ^{10}B delivered to the cells and thus several classes of BNCT agents have been developed in the past such as sodium tetraborate (borax), sodium pentaborate, *p*-boronophenylalanine (BPA), sodium borocaptate (BSH), *p*-carboxyphenylboronic acid, or sodium decahydrodecaborate.[15–18] However, the need for the delivery of high amounts of ^{10}B led to the development of boron clusters (boranes, carboranes and metallacarboranes).[19] In dicarba-*closo*-dodecarboranes, hexacoordinated carbon and boron atoms adopt the regular icosahedral geometry. As discussed above, the two carbon vertices in dicarba-*closo*-dodecarboranes bear relatively acidic hydrogen atoms, which are readily replaced by metals or organic groups.[20,21] Besides, substituents can also be introduced with good control to at least a certain number of boron vertices, making the research in this area very versatile and attractive for BNCT. The icosahedral *closo*-$C_2B_{10}H_{12}$ carborane[22] and metallacarborane[23] $[M(C_2B_9H_{11})_2]^-$ clusters are 3D aromatic moieties, possessing high symmetry and stability,[24] and generally low cytotoxicity,[25,26] being good candidates for BNCT.[25,27–29] In this frame, several compositions for potential BNCT applications have been developed,[30–35] including high boron-loaded DNA-oligomers,[36] periphery-decorated and core-initiated borane polyanionic macromolecules,[37] peptide–cobalt bis(dicarbollide) conjugates,[38] nucleoside–boron cluster conjugates[39,40] and cholesterol–metallacarborane conjugates,[41] among others.

Examples of ruthenacarborane complexes for potential BNCT are scarcer and comprise the 'Ru(η^6-arene)' moiety[42–46] bonded to the carborane through a dithiolate motif or the upper pentagonal face of the cluster. In this frame, taking into consideration the high stability and the cytotoxic properties of $[Ru(\eta^5\text{-}C_5H_5)(2,2'\text{-bipyridine})(Z)]^+$ complexes we decided to replace the $(\eta^5\text{-}C_5H_5)^-$ ligand by the bioisostere dicarbollide anion. The cytotoxicity of the $[Ru(\eta^5\text{-}C_5H_5)(2,2'\text{-bipyridine})(Z)]^+$ family of compounds can be tuned by the ligand Z; when Z is a phosphane, the compounds are highly cytotoxic, whereas when Z is a CO, the compounds show only moderate to low cytotoxicity.[47] Previous studies also showed that $[Ru(\eta^5\text{-}C_5H_5)(2,2'\text{-bipyridine})(Z)]^+$ compounds are well internalized into cancer cells.[48–50] Thus, based on previous results, we decided to synthesize two multifunctional compounds with the general formula [3-CO-3,3-{κ^2-4,4′-R_2-2,2′-bipy}-*closo*-3,1,2-$RuC_2B_9H_{11}$], that would provide multi-modal treatment acting at once as chemotherapeutic and BNCT agents. The potential treatment using bifunctional compound types would allow to reduce the doses to get the same therapeutic effect while diminishing the secondary effects to the patient.

Results and discussion

Synthesis

New mononuclear ruthenium–carboranyl complexes bearing bipyridyl derivatives with the general formula [3-CO-3,3-{κ^2-4,4′-R_2-2,2′-bipy}-*closo*-3,1,2-$RuC_2B_9H_{11}$] were obtained by treatment of the parental tricarbonyl complex [3,3,3-$(CO)_3$-*closo*-3,1,2-$RuC_2B_9H_{11}$] with trimethylamine N-oxide (Me_3NO, TMAO) following a reported procedure,[51] and the corresponding bipyridyl ligand (Scheme 1, **RuCB1**, R = –CH_3; **RuCB2**, R = –CH_2OH). Sigma coordination of each bidentate chelator to the ruthenium core was achieved in comparable yield to previously reported *closo*-ruthenacarboranes bearing bipyridine based ligands.[51]

Purification of the new *closo*-ruthenacarborane complexes was achieved by column chromatography on silica gel and single crystals of **RuCB1** and **RuCB2** were successfully obtained by slow diffusion recrystallization, at room temperature.

The formulation and purity of the new complexes was fully elucidated, both in the solid-state and in solution, by FT-IR, UV-Vis and NMR (^{1}H, ^{11}B, ^{13}C nuclei) spectroscopies, cyclic voltammetry and single-crystal X-ray diffraction.

NMR spectroscopy

Tables S1 and S2 at the ESI† summarize the ^{1}H NMR and ^{11}B $\{^1H\}$ NMR data for **RuCB1** and **RuCB2**. All resonances were attributed using 1D and 2D NMR experiments (^{1}H, ^{11}B, $^{13}C\{^1H\}$, ^{1}H–^{1}H COSY, HMQC, and HMBC) following the atom numbering presented in Scheme 1. The newly synthesized *closo*-ruthenacarborane complexes displayed resonances in their ^{1}H NMR spectra that were easily ascribed to the two CH cage protons due to their broad character. These signals appeared at δ 3.26 ppm and δ 3.30 ppm for **RuCB1** and **RuCB2**, respectively, and revealed an integration ratio of 1 : 1 between the carboranyl ligand and the respective 2,2′-bipyridyl ligand. The bipyridyl aromatic protons resonate at higher chemical shift (downfield)

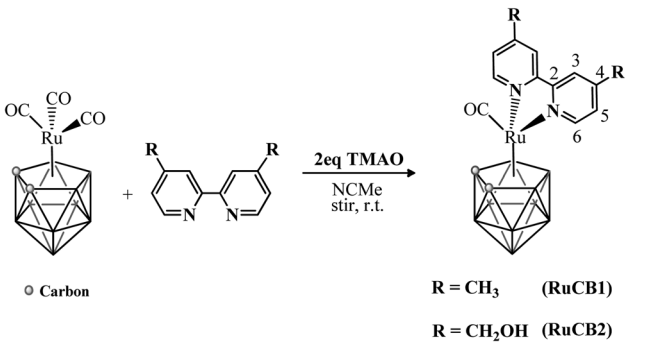

Scheme 1 Synthetic route of the new ruthenacarborane complexes RuCB1 and RuCB2; the 2,2′-bipyridine ligand is numbered for NMR assignments. TMAO = trimethylamine N-oxide.

values when compared to the corresponding resonances of the free ligand (**RuCB1**: ΔH_6 +0.49 ppm, ΔH_5 +0.34 ppm and ΔH_3 +0.26 ppm; **RuCB2**, ΔH_6 +0.49 ppm, ΔH_5 +0.31 ppm and ΔH_3 +0.14 ppm; see Table S1†) which agrees with a σ dative coordination to the metal. Additionally, a resonance at δ 2.62 ppm appears in the ^{1}H NMR of complex **RuCB1** and it is readily attributed to the equivalent protons of the methyl groups of the coordinated 4,4′-dimethyl-2,2′-bipyridyl ligand, while the two geminal protons of the groups of the 4,4′-dihydroxymethyl-2,2′-bipyridyl ligand of complex **RuCB2** resonate at δ 4.96 ppm. Characterization of these complexes was also performed by ^{13}C-APT NMR experiments and the results are in accordance with the previously discussed effects in the ^{1}H NMR analysis. In the ^{13}C-APT NMR spectra of all complexes, a broad singlet resonance appears at $\delta \approx 45$ ppm and by their position and shape, were easily attributed to the two equivalent carbons present at the carboranyl structure. The resonances for the carbonyl co-ligand appear at δ 199 ppm along with the expected remaining carbons of the 2,2′-bipyridyl ligand ($121 < \delta < 156$ ppm).

RuCB1 and **RuCB2** displayed at its ^{11}B{^{1}H} NMR spectra, a general pattern of four peaks with an integration intensity ratio of 1 : 3 : 2 : 3 (Fig. S4;† spectra from **RuCB1**), being the second and fourth signals result of overlap of broad unresolved 1 + 2 resonances, similarly to results reported for [3-CO-3,3-{κ^2-$Me_2N(CH_2)_2NMe_2$}-*closo*-3,1,2-$RuC_2B_9H_{11}$].[51] The appearance of the aforementioned resonances agrees with the typical chemical shift range for the *closo*-3,1,2-$MC_2B_9H_{11}$ system (M = Rh, Ru) (-0.9 ppm $> \delta > -22.3$ ppm).[52–55] Furthermore, the weighted average ^{11}B NMR chemical shift, $\langle\delta(^{11}B)\rangle$, is -11.1 and -12.4 ppm for **RuCB1** and **RuCB2**, respectively that were higher than -10 ppm and agree with a *closo* metallacarborane cluster.[56–58] In addition, the $^1J_{HB}$ higher than 100 Hz were found in the ^{11}B NMR spectra giving a clear indication that all B–H protons from the $C_2B_9H_{11}$ cage remain intact.

The sensitivity of the electron distribution in *closo* icosahedral carborane/metallacarborane derivatives due to the presence of substituents at the vertexes is well known.[59,60] The averaged chemical shift values move upfield (Table S1†) when the ligand is bipyridyl indicating shielding of the cluster in the *closo* ruthenacarboranes **RuCB1** and **RuCB2** relatively to its precursor [3,3,3-$(CO)_3$-*closo*-3,1,2-$RuC_2B_9H_{11}$] ($\langle\delta\rangle$ -7.7 ppm). This result correlates well with the CH_{cage} resonances in the ^{1}H NMR that are shifted upfield in the *closo* ruthenacarboranes **RuCB1** and **RuCB2** relatively to the tricarbonyl starting complex (δ 4.15 ppm).

The general shielding effect observed for the cage and the carbonyl nuclei resonances combined with the confirmed deshielding of the 2,2′-bipyridyl protons gives clear evidence of electron flow from the 2,2′-bipyridyl through the ruthenium center towards the boron cage and the carbonyl co-ligand. The presence of a more donating group at the 2,2′-bipyridine substituent improves the electronic flow to the carboranyl moiety.

FT-IR spectroscopy

The FT-IR spectra of the *closo*-ruthenacarborane complexes presented the characteristic bands of the carboranyl moiety ($\nu_{C-H,stretching} \sim 3040$ cm^{-1} and $\nu_{B-H,stretching} \sim 2550$ cm^{-1}), the bipyridyl derivatives ligands (*ca.* 1520–1400 cm^{-1} and at ~2960 cm^{-1} for $\nu_{C-H,stretching}$) and a single absorption band attributed to the vibrational frequency of the metallic carbonyl (approximately at 1960 cm^{-1}). It is also noticeable the presence of the stretching frequency of the alcohol functional group in complex **RuCB2** spectrum ($\nu_{O-H,stretching} \sim 3310$ cm^{-1}). The carbonyl bonded to the metal center is coordinated in an almost linear fashion (confirmed by crystallographic data) and its binding to the ruthenium ion can be explained by two synergetic contributions: σ-donation from the ligand to the metal and π-back donation from the metal to the ligand. This type of interaction between the orbitals of the metal and the ligand led, in both cases, to a negative shift of the $\nu_{C\equiv O}$ (av. -93 cm^{-1}).

UV-Vis spectroscopy

The optical absorption spectra of the ruthenacarborane complexes were recorded using 1.0×10^{-5} to 1.0×10^{-6} M solutions in dichloromethane and dimethyl sulfoxide (Table S3†). The trend observed in the electronic absorption spectra of both complexes follows the same pattern and Fig. 1 is representative of their behavior. Despite the strong absorption bands characteristic of each bipyridyl derivative and the {Ru(CO)($C_2B_9H_{11}$)} organometallic fragment (appearing below 300 nm), typical electronic spectra of these compounds are characterized by two broad, medium-strength absorption bands appearing in the range of 330 to 530 nm. The solvatochromic effect observed at the medium-strength transitions of complex **RuCB2** showed that these bands are blue-shifted with the increase of the polarity of the solvent (368 nm in CH_2Cl_2 *vs.* 347 nm in DMSO for the stronger absorption; 453 nm in CH_2Cl_2 *vs.* 434 nm in DMSO for the weaker absorption). Based on their position, intensity and similar behavior in related compounds, we can attribute them as charge transfer (presumably ligand to metal charge transfer) and d–d transitions.[51]

Electrochemical studies

The electrochemical behavior of organometallic ruthenacarborane complexes was studied by cyclic voltammetry in

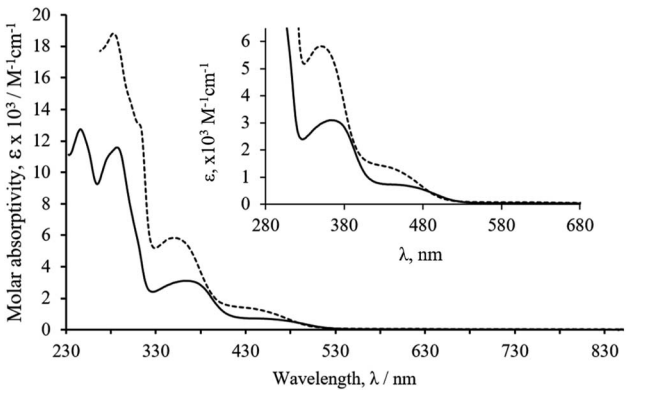

Fig. 1 Electronic spectra of complex **RuCB2** in dichloromethane (full line) and dimethylsulfoxide (dotted line). Expansion of the spectra in the LMCT region.

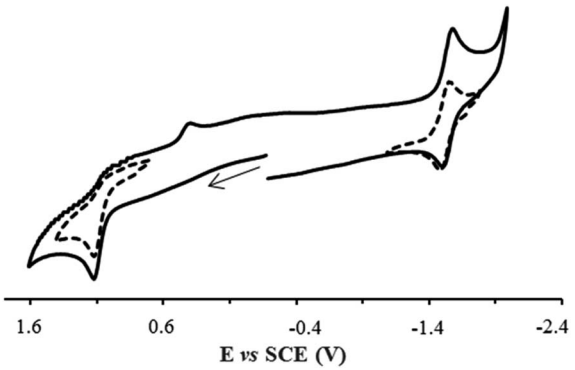

Fig. 2 Cyclic voltammogram of complex **RuCB1** in acetonitrile, at 100 mV s^{-1}, showing the reversibility of the isolated redox processes (dashed lines).

acetonitrile and dichloromethane solutions using ammonium hexafluorophosphate as supporting electrolyte (Table S4, see ESI†). Complex **RuCB1** (Fig. 2) showed an irreversible oxidation process (E_{pa} = 1.12 V in both solvents) that retains its irreversibility when isolated and studied at different scan rates. This behaviour suggests a rapid irreversible chemical reaction following the electron transfer process, attributed to the ruthenium centre, in accordance with the literature data for similar complexes.[51] Along with this oxidative process, and after scanning for negative potentials, two other reductive processes appeared (E_{pc} = −1.45 V and $E_{1/2}$ = −1.54 V in acetonitrile), being the first irreversible and the second quasi-reversible. These processes can be addressed to the bipyridyl ligand as previously reported for related ruthenium–cyclopentadienyl complexes[47] or to a reduction in the ruthenium centre as stated before for similar complexes.[51,61] Complex **RuCB2** showed a similar behavior in both solvents. Considering the potentials attributed to the Ru^{II}/Ru^{III} redox pair for these compounds and the absence of oxidation processes for the analogue [Ru(η^5-C_5H_5)(CO)(bipy)][CF_3SO_3], in the same experimental conditions,[47] one can conclude that the presence of the carboranyl ligand facilitates the oxidation of the metal center, as it was expected by the ability of higher oxidation states stabilization characteristic of the [*nido*-7,8-$C_2B_9H_{11}$]$^{2-}$ ligand.[60]

Single crystal X-ray diffraction of complexes RuCB1 and RuCB2

Single crystal suitable for X-ray diffraction studies were obtained from slow evaporation of acetone (**RuCB1**) or slow diffusion of hexane solutions into tetrahydrofuran solution (**RuCB2**) to give an orange to yellow needle-shaped crystals suitable for X-ray diffraction analysis. The molecular structures obtained are shown in Fig. 3, and selected distances and angles and representative crystallographic data are given at Tables 1 and S5.†

Complex **RuCB1** crystallizes in the monoclinic system, space group $P2_1/c$ whereas complex **RuCB2** crystallizes in the monoclinic system, space group $P2_1/n$. In the crystallographic studies, it was possible to see that the basic structural skeleton of this type of complexes is the expected three-legged piano stool structure. Each correspondent crystallographic data revealed that the presence of the 2,2′-bipyridyl derivatives does not affect the full engagement of the C_2B_3 face of the carboranyl ligand towards the ruthenium center, once it remains coordinated in its pentahapto fashion. No evidence of cage slippage or distortion between the carbon atoms of the carboranyl was noticed for any of the complexes. In addition to the fully-coordinated planar 2,2′-bipyridyl ligand (C(1)–C(2) 1.658 Å, Ru–C_{cage} (average) 2.196 Å, Ru–B (average) 2.240 Å for complex **RuCB1**, and C(1)–C(2) 1.642 Å, Ru–C_{cage} (average) 2.200 Å, Ru–B (average) 2.456 Å for complex **RuCB2**) there is the lone carbonyl co-ligand, bounded in the expected linear form.

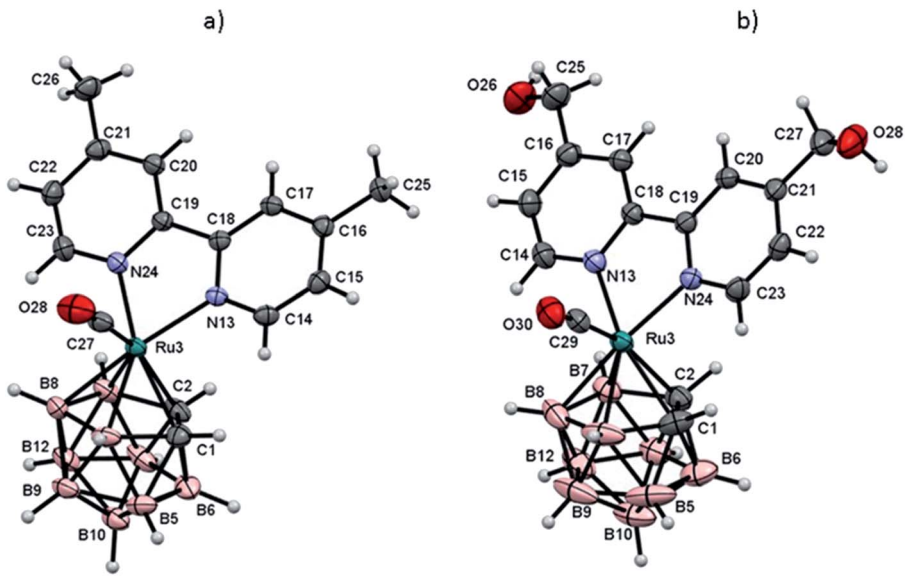

Fig. 3 ORTEP representation of complex **RuCB1** (a) and **RuCB2** (b). The disordered of –OH groups have been omitted for clarity.

Table 1 Selected bond lengths (Å) and angles (deg) for **RuCB1** and **RuCB2**

	RuCB1	RuCB2
Ru(3)–C(1)	2.174(2)	2.179(3)
Ru(3)–C(2)	2.218(2)	2.220(3)
Ru(3)–C(27)	1.863(2)	—
Ru(3)–C(29)	—	1.865(3)
Ru(3)–N(13)	2.1317(17)	2.104(2)
Ru(3)–N(24)	2.1018(18)	2.125(2)
Ru(3)–B(4)	2.214(3)	2.210(4)
Ru(3)–B(7)	2.247(3)	2.239(4)
Ru(3)–B(8)	2.266(3)	2.272(4)
C(1)–C(2)	1.658(3)	1.642(5)
C(27)–Ru(3)–N(13)	94.12(9)	—
C(27)–Ru(3)–N(24)	91.04(9)	—
C(27)–Ru(3)–C(1)	114.93(10)	—
C(27)–Ru(3)–C(2)	158.44(10)	—
C(29)–Ru(3)–N(13)	—	91.61(12)
C(29)–Ru(3)–N(24)	—	91.17(11)
C(29)–Ru(3)–C(1)	—	114.10(14)
C(29)–Ru(3)–C(2)	—	157.52(13)

The crystal structure of **RuCB2** reveals two orientations of molecules (head-to-tail) arranged in infinite double zig-zag chains running parallel to the *c* crystallographic axis (Fig. 4). The two carborane B–H vertices located at the B_5 plane that are *trans* to the two carbon cluster atoms participate in the B–H···O–H intermolecular interactions. These intermolecular B–H···H–O interactions are strong since the contacts are shorter than the sum of the van der Waals radii minus 0.70 Å.[62]

Stability studies in aqueous media

The behavior of the compounds in cellular media was evaluated to infer about their stability in similar conditions to the biological assays. The study was performed by UV-Vis spectroscopy during 24 h (Fig. S11†). The UV-Vis absorption spectra of the complexes in 3% DMSO/97% DMEM exhibit one strong absorption band in the UV range and two broad absorptions in the visible range, similar to the correspondent spectra observed in organic solvents. Variations lower than 10% over the 24 hours challenge for complex **RuCB1** and **RuCB2** were observed, supporting that the original three-legged piano-stool geometry is kept over the assay time.

Biological assays

Analysis of the cytotoxicity in cancer cell lines

The cytotoxic activity of **RuCB1** and **RuCB2** was determined by the colorimetric MTT assay in melanoma (A375) and glioblastoma (U87) cancer cell lines. These cell lines were selected considering that this type of tumors have shown favorable clinical responses with BNCT.[63] As indicated in Table 2, after 24 h of treatment with **RuCB1** no cytotoxic activity up to 100 μM was observed and **RuCB2** showed moderate activity for both cell lines, although more active in the glioblastoma cells. These results indicate that these compounds show the potential to be further explored regarding their boron accumulation in cancer cells.

Intracellular distribution of the ruthenium complexes

The intracellular distribution of the complexes **RuCB1** and **RuCB2** was performed using A375 cells following exposure to each complex for 24 h at a concentration equivalent to their IC_{50} values (for compound **RuCB1** a concentration of 100 μM was used). Cytosol, membrane, nucleus, and cytoskeletal fractions were extracted using a commercial kit as described in the Experimental section. One can observe, the different substituents at the bipyridine lead to different accumulation patterns (^{10}B and ^{102}Ru quantification) (Fig. 5). While the methylated compound **RuCB1** is distributed through cytoskeleton, membranes, and nucleus, the hydroxymethylated compound **RuCB2** is mainly accumulated at the membrane of cells (~90%). It is interesting to observe that **RuCB2** keeps the $^{10}B/^{102}Ru$ ratio unchangeable in all cell compartments indicating that probably the Ru–carborane moiety is stable. However, **RuCB1** shows considerable differences indicating that, at some point after internalization, the Ru is detached from the carborane. For

Table 2 IC_{50} values (μM) for complexes **RuCB1** and **RuCB2**, at 24 h incubation, in A375 and U87 cancer cells

Compounds	A375	U87
RuCB1	>100	107 ± 46
RuCB2	57.0 ± 1.8	25.5 ± 8.3

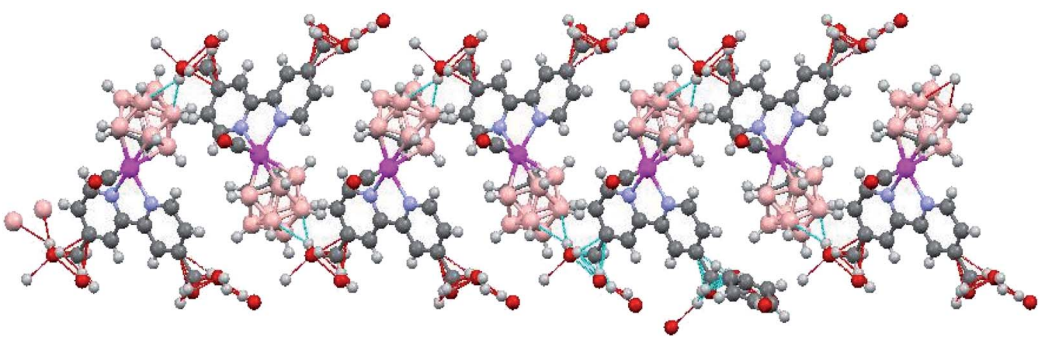

Fig. 4 Crystal structure of complex **RuCB2** showing the B–H···H–O dihydrogen bonding which results in a head to tail arrangement of molecules forming an infinite double zig-zag chain running parallel to the *c* crystallographic axis.

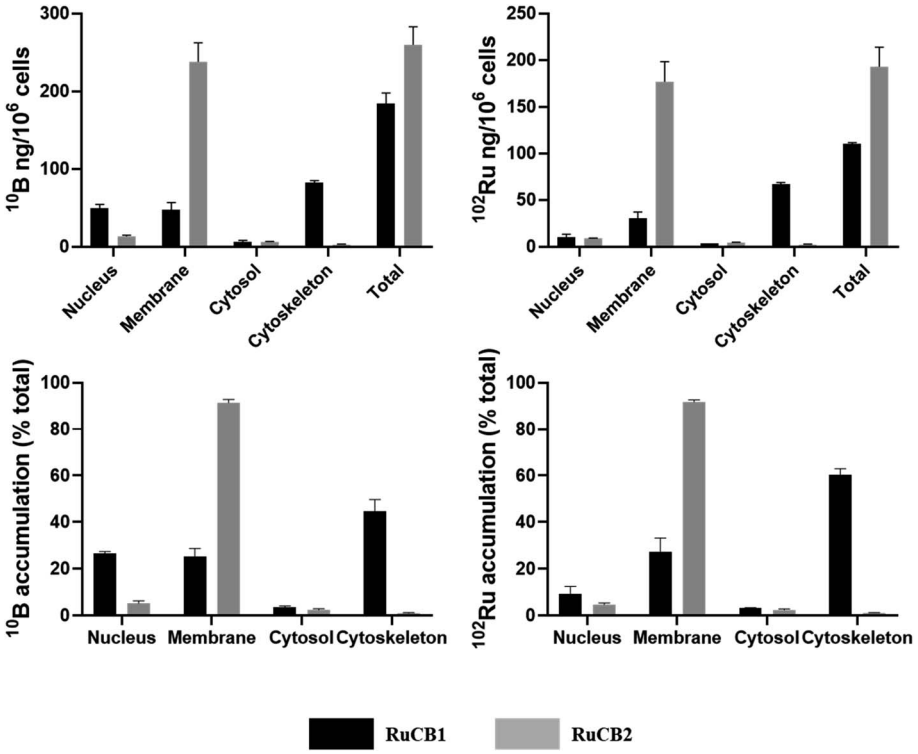

Fig. 5 Cellular ^{10}B and ^{102}Ru distribution in A375 cells treated with compounds **RuCB1** and **RuCB2** at a concentration equivalent to their IC_{50} values found at 24 h challenge. Results are expressed in ng of ^{10}B and ^{102}Ru per million of cells (top) or in total percentage (bottom). Results are expressed as mean ± SD of two independent experiments.

Table 3 Amount of B internalized in A375 cells, determined by ICP-MS

Incubated **RuCB2** (μM)	Internalized B (μg g^{-1})	Internalized ^{10}B μg g^{-1} to perform BNCT[a]
19	71	14
37	137	27
74	250	50

[a] ^{10}B μg g^{-1} were calculated from its natural abundance (20%).

RuCB1, the main difference is observed at the nucleus, where the ^{10}B/^{102}Ru ratio increases by ~3-fold.

Normalizing the results to the administered doses of compounds, **RuCB2** uptake is 2.6-fold higher than **RuCB1** (^{10}B and ^{102}Ru quantification).

For BNCT to be successful, enough ^{10}B should be delivery to the tumor cells. Therefore, experiments were conducted to determine the amount of B that was taken up by the cells as a function of the concentrations of the two compounds.

As shown in Fig. S12,† the most promising compound seems to be **RuCB2** since it is the compound presenting higher boron internalization that is proportional to the concentration used (Table 3). Even if the boron internalized by cells is not enriched in ^{10}B, the amount internalized is enough to perform BNCT on cells.[64,65] On the contrary, **RuCB1** has a low B accumulation within cells, reaching a threshold at ~30 μM. These results indicate that **RuCB2** is a potential candidate to be evaluated as a BNCT agent.

Conclusion

Two new ruthenium carboranyl complexes with 2,2′-bipyridine derivatives were synthesized and characterized by several analytical and spectroscopic techniques. Both compounds crystallize in the monoclinic system, showing the expected three-legged piano stool structure.

The compounds' cytotoxicity was evaluated in melanoma (A375) and glioblastoma (U87) cell lines showing low to moderate cytotoxicity. Their uptake into A375 cells was determined *via* ^{10}B and ^{102}Ru quantification by ICP-MS showing that **RuCB2**, bearing a hydroxymethyl group at the bipyridine, fulfills the prerequisites to be further evaluated as a potential bimodal agent (chemo + radiotherapy). As far as we know, this is the first time that a ruthenacarborane bearing 2,2′-bipyridine derivatives has been considered for this application.

Experimental section

General procedures

All reactions and manipulations were performed under nitrogen atmosphere using Schlenk techniques. All solvents used were dried and freshly distilled under nitrogen before use, using standard methods. The carboranyl ligand ($C_2B_9H_{13}$) and the [3,3,3-(CO)$_3$-*closo*-3,1,2-$RuC_2B_9H_{11}$] precursor were synthesized as described in the literature.[7,66] ^{1}H, ^{11}B, and ^{13}C and NMR spectra were recorded on a Bruker Avance 400 spectrometer at probe temperature using commercially available deuterated

acetone. ^{1}H and ^{13}C chemical shifts (s = singlet; d = duplet; t = triplet; m = multiplet; comp = complex) are reported in parts per million (ppm) downfield from internal standard Me_4Si and the ^{11}B and $^{11}B\{^{1}H\}$ NMR spectra are reported in ppm downfield from external standard $BF_3 \cdot OEt_2$. Coupling constants are reported in Hz. All assignments were attributed using DEPT-135, COSY, HMBC, and HMQC NMR techniques. Infrared spectra were recorded on KBr pellets using a Mattson Satellite FT-IR spectrophotometer. Only considered relevant bands were cited in the text. Electronic spectra were obtained at room temperature on a Jasco V-660 spectrometer from solutions of 10^{-4} to 10^{-6} M in quartz cuvettes (1 cm optical path). Elemental analyses were performed at Laboratório de Análises, at Instituto Superior Técnico, using a Fisons Instruments EA1 108 system. Data acquisition, integration and handling were performed using a PC with the software package EAGER-200 (Carlo Erba Instruments).

Syntheses

[3-CO-3,3-{κ^2-4,4′-$(CH_3)_2$-2,2′-bipy}-*closo*-3,1,2-$RuC_2B_9H_{11}$] (RuCB1). [3,3,3-$(CO)_3$-*closo*-3,1,2-$RuC_2B_9H_{11}$] (0.20 g, 0.63 mmol) was combined with 1 equivalent of 4,4′-dimethyl-2,2′-bipyridine (0.10 g, 0.63 mmol) and 2 equivalents of Me_3NO (0.10 g, 1.26 mmol) in a Schlenk and MeCN (40 mL) was added to the reactants. The reaction mixture was stirred for 24 hours at room temperature. After that, the solvent was removed in vacuum and the residue obtained was chromatographed in silica gel using as eluent a mixture of dichloromethane and *n*-hexane (4 : 1). Extraction yielded a bright canary yellow band that was removed from the column with an increased proportion of the *n*-hexane phase. After removing all the yellow fraction, the solvent was removed by vacuum. The residue obtained was recrystallized by slow diffusion of *n*-hexane in dichloromethane. Yellow needle-shaped single crystals of **RuCB1** were obtained from slow evaporation of an acetone solution, under air.

Yield: 24%; yellow needle-shaped single crystals, recrystallized from dichloromethane/*n*-hexane. ^{1}H NMR [$(CD_3)_2CO$, Me_4Si, δ/ppm]: 9.00 (d, 2H, $^{3}J_{HH} = 5.6$, H_6), 8.56 (s, 2H, H_3), 7.56 (d, 2H, $^{3}J_{HH} = 5.2$, H_5), 3.26 (s, 2H, CH_{cage}), 2.62 (s, 6H, CH_3). APT $^{13}C\{^{1}H\}$ NMR [$(CD_3)_2CO$, Me_4Si, δ/ppm]: 198.7 (CO), 156.2 (C_2), 155.5 (C_6), 151.8 (C_4), 128.4 (C_5), 124.9 (C_3), 44.9 (br, C_{cage}), 21.2 (CH_3). ^{11}B NMR [$(CD_3)_2CO$, δ/ppm]: −0.9 (d, 1B, $^{1}J_{BH}$ = 129.0), −7.3 (m, 5B), −20.9 (d, 3B, $^{1}J_{BH}$ = 150.2). FTIR [KBr pellets, cm^{-1}]: 2960–2850 cm^{-1} (ν_{C-H}), 2549 cm^{-1} (ν_{B-H}), 1967 cm^{-1} ($\nu_{C\equiv O}$). UV-Vis in CH_2Cl_2 [λ_{max}/nm ($\varepsilon \times 10^3$/M^{-1} cm^{-1})]: 246 (11.28), 287 (10.25), 311 (Sh), 362 (2.74), 451 (0.60). UV-Vis in DMSO [λ_{max}/nm ($\varepsilon \times 10^3$/M^{-1} cm^{-1})]: 283 (18.71), 311 (13.01), 350 (5.80), 438 (1.35). Elemental analysis [calculated for **RuCB1** $\frac{1}{4}CH_2Cl_2$] found (calculated): C 39.1 (39.2), H 5.2 (5.1), N 5.5 (6.0).

[3-CO-3,3-{κ^2-4,4′-$(CH_2OH)_2$-2,2′-bipy}-*closo*-3,1,2-$RuC_2B_9H_{11}$] (RuCB2). [3,3,3-$(CO)_3$-*closo*-3,1,2-$RuC_2B_9H_{11}$] (0.20 g, 0.63 mmol) was combined with 1 equivalent of 4,4′-dihydroxymethyl-2,2′-bipyridine (0.13 g, 0.63 mmol) and 2 equivalents of Me_3NO (0.10 g, 1.26 mmol) in a Schlenk and MeCN (40 mL) was added to the reactants. The reaction mixture was stirred for 24 hours at room temperature. After that period, the solvent was removed by vacuum and the residue obtained was chromatographed in silica gel using as eluent a mixture of dichloromethane and methanol (2 : 0.2). Elution yielded a dark orange band that was removed from the column gradually. Then all the pure fractions were collected and the solvent was removed by vacuum. The residue obtained was recrystallized by slow diffusion of *n*-hexane in tetrahydrofuran affording light orange needle-shaped single crystals of **RuCB2**.

Yield: 19%; orange needle-shaped single crystals, recrystallized from tetrahydrofuran/*n*-hexane. ^{1}H NMR [$(CD_3)_2CO$, Me_4Si, δ/ppm]: 9.09 (d, 2H, $^{3}J_{HH} = 5.6$, H_6), 8.64 (s, 2H, H_3), 7.70 (d, 2H, $^{3}J_{HH} = 5.6$, H_5), 5.05 (t, 2H, $J_{HH} = 5.6$, OH), 4.96 (d, 4H, $J_{HH} = 4.8$, CH_2OH), 3.30 (s, 2H, CH_{cage}). APT $^{13}C\{^{1}H\}$ NMR [$(CD_3)_2CO$, Me_4Si, δ/ppm]: 198.5 (CO), 156.2 (C_2), 156.1 (C_4), 155.7 (C_6), 124.6 (C_5), 121.0 (C_3), 62.7 (CH_2OH), 44.9 (br, C_{cage}). ^{11}B NMR [$(CD_3)_2CO$, δ/ppm]: −2.1 (d, 1B, $^{1}J_{BH} = 129.0$), −8.6 (m, 5B), −22.3 (d, 3B, $^{1}J_{BH}$ = 150.2). FTIR [KBr pellets, cm^{-1}]: 3310 cm^{-1} (ν_{O-H}), 2920–2850 cm^{-1} (ν_{C-H}), 2520 cm^{-1} (ν_{B-H}), 1950 cm^{-1} ($\nu_{C\equiv O}$). UV-Vis in CH_2Cl_2 [λ_{max}/nm ($\varepsilon \times 10^3$/M^{-1} cm^{-1})]: 245 (18.92), 289 (16.84), 314 (Sh), 368 (4.33), 453 (1.07). UV-Vis in DMSO [λ_{max}/nm ($\varepsilon \times 10^3$/M^{-1} cm^{-1})]: 284 (16.06), 313 (10.45), 347 (4.32), 434 (1.08). Elemental analysis [calculated for **RuCB2** $\frac{1}{4}$THF found (calculated)]: C 38.8 (38.8), H 5.1 (5.1), N 5.1 (5.7).

Electrochemical studies

The electrochemical experiments were performed with an EG&G Princeton Applied Research Model 273A potentiostat/galvanostat and controlled by a personal computer using Electrochemistry PowerSuite v2.51 data acquisition software from Princeton Applied Research. Cyclic voltammograms were obtained in solutions of $[NBu_4][PF_6]$ in acetonitrile (0.1 M) or dichloromethane (0.2 M) at room temperature using a three-electrode configuration with a platinum-disk working electrode (1.0 mm diameter) probed by a Luggin capillary connected to a silver-wire pseudo-reference electrode; a Pt wire auxiliary electrode was employed. The redox potentials of the complexes were measured in the presence of ferrocene as the internal standard and the redox potential values are normally quoted relative to the ferrocene/ferrocenium redox couple ($E_{1/2} = 0.40$ V and 0.46 V *vs.* SCE for acetonitrile and dichloromethane, respectively). The solutions were purged with nitrogen and kept under an inert atmosphere throughout the measurements. Reagent grade solvents were dried, purified by standard procedures and distilled under nitrogen atmosphere before use.

X-ray structure analysis

The measurements were carried out on a BRUKER SMART APEX CCD diffractometer using graphite-monochromated Mo Kα radiation (λ = 0.71073 Å) from an X-ray Tube. For **RuCB1** the measurement was made in the range 1.836 to 28.363° for θ. Hemi-sphere data collection was carried out with ω and φ scans. A total of 13 262 reflections were collected of which 4534 [R(int) = 0.0272] were unique.

For **RuCB2** the measurement was made in the range 2.237 to 28.386° for θ. Full-sphere data collection was carried out with ω and φ scans. A total of 35 439 reflections were collected of which 5582 [R(int) = 0.0317] were unique.

The structures were solved by the dual-space algorithm and refined by full-matrix least-squares methods on F^2. The non-hydrogen atoms were refined anisotropically. The H-atoms were placed in geometrically optimized positions and forced to ride on the atom to which they are attached, except the carborane B–H and C–H, which were located in the difference Fourier map and refined freely.

The C atoms in the carborane were located using the VCD and BHD methods.[67,68]

For **RuCB2** a considerable amount of electron density attributable to half a disordered THF solvent molecule per asymmetric unit was removed with the SQUEEZE option of PLATON.[69] Those solvent molecules are, however, included in the reported chemical formula and derived values (*e.g.* formula weight, F(000), *etc.*).

Programs used: data collection, Smart;[70] data reduction, Saint+;[71] absorption correction, SADABS.[72,73] Structure solution and refinement was done using SHELXT – SHELXL.[74,75]

Stability studies

For the stability studies, both complexes were dissolved in 100% DMSO and a sample containing each compound in 3% DMSO/97% DMEM at *ca.* 200 μM was prepared. Their electronic spectra were recorded in the range allowed by the solvent mixture at set time intervals. The samples used were protected from light sources and stored at room temperature between measurements.

Cytotoxic activity

The cytotoxic activity of the tested compounds was determined in melanoma A375 and glioblastoma U87 cancer cell lines obtained from ATCC, using the colorimetric MTT (3-(4,5-dimethylthiazol-2-yl)-2,5-diphenyltetrazolium bromide) assay. Both cell lines were grown in DMEM-GlutamaxI medium supplemented with 10% FBS and maintained in a humidified incubator at 37 °C (Heraeus, Germany) with 5% CO_2. In a typical assay, cells (1–2 × 10^4 cells per well) were seeded into 96 well plates and allowed to adhere overnight. Then, cells were treated with crushed dried crystalline samples of the compounds, first diluted in DMSO for complete solubilization, and then in medium to prepare serial dilutions within the concentration range of 0.1–100 μM. After 24 h incubation, the medium was discarded and 200 μL of MTT solution in PBS (0.5 mg mL^{-1}) were added to each well. After 3 h at 37 °C, the MTT solution was removed and replaced by DMSO (200 μL) to solubilize the formazan crystals formed. The percentage of cellular viability was assessed measuring the absorbance at 570 nm using a plate spectrophotometer (Power Wave Xs, Bio-Tek). The IC_{50} values were calculated using the GraphPad Prism software (version 5.0). Results are shown as the mean ± SD of at least two independent experiments done with six replicates each.

Cellular uptake measured by ICPMS analysis

For the cellular uptake experiments, A375 human melanoma cells (*ca.* 1 × 10^6 cells/5 mL) were seeded into t25 flasks and allowed to adhere overnight in a 5% CO_2 incubator at 37 °C. Cells settled for 24 h, followed by the addition of **RuCB1** and **RuCB2**, at a concentration equivalent to their IC_{50} values found for 24 h challenge at 37 °C. After incubation, cells were washed with ice-cold PBS and treated in order to obtain a cellular pellet. The cytosol, membranes/particulate, cytoskeletal and nuclear fractions were extracted using a FractionPREP™ (BioVision, USA) cell fractionation kit according to the manufacturer's protocol. The Ru (^{102}Ru) and B (^{10}B) content in each fraction was measured by a Thermo X-Series Quadrupole ICPMS (Thermo Scientific) after digestion of the samples and using a procedure similar to a previously described.[76]

Internalization studies as a function of the concentration

A375 human melanoma cells were seeded in 6 cm diameter dishes. After 24 h, cells were incubated for 24 h with increasing concentrations of **RuCB1** and **RuCB2**. At the end of the incubation, cells were washed three times with PBS and detached with trypsin/EDTA. A375 cells were resuspended in 200 μL of PBS, sonicated for 30″ at 30% power in ice and their protein concentration was measured by the Bradford method. Boron amount [μg g^{-1}] in each cell sample was evaluated by Inductively Coupled Mass Spectrometry (ICP-MS) (Element-2; Thermo-Finnigan, Rodano (MI), Italy) at medium mass resolution. Sample digestion was performed with 1 mL of concentrated HNO_3 (70%) using a high-performance Microwave Digestion System (ETHOS UP Milestone, Bergamo, Italy). A natural abundance B standard solution was analyzed during sample runs in order to check changing in the systematic bias. The calibration curve was obtained using four B absorption standard solutions (Sigma-Aldrich) in the range 0.2–0.01 μg mL^{-1}.

Conflicts of interest

There are no conflicts to declare.

Acknowledgements

Centro de Química Estrutural and Centro de Ciências e Tecnologias Nucleares acknowledge Fundação para a Ciência e Tecnologia (FCT) for the Projects UIDB/00100/2020 and UID/MULTI/04349/2013, respectively. This work was also funded in the scope of the project PTDC/QUI-QIN/28662/2017 (FCT). R. G. Teixeira thanks FCT for his Ph.D. Grant (SFRH/BD/135830/2018). A. Valente acknowledges the CEECIND 2017 Initiative (CEECIND/01974/2017) and the COST Actions 17104 STRATAGEM and CM1302 (SIPs) (European Cooperation in Science and Technology). C. Viñas thanks MINECO (CTQ2016-75150-R) and Generalitat de Catalunya (2017 SGR 1720) for the financial support.

References

1 P. Zhang and P. J. Sadler, Advances in the design of organometallic anticancer complexes, *J. Organomet. Chem.*, 2017, **839**, 5–14.

2 L. Zeng, P. Gupta, Y. Chen, E. Wang, L. Ji, H. Chao and Z. S. Chen, The development of anticancer ruthenium(II) complexes: From single molecule compounds to nanomaterials, *Chem. Soc. Rev.*, 2017, **46**(19), 5771–5804.

3 R. N. Grimes, *Carboranes*, Elsevier Inc., 3rd edn, 2016, p. 1058.

4 D. Olid, R. Núñez, C. Viñas and F. Teixidor, Methods to produce B–C, B–P, B–N and B–S bonds in boron clusters, *Chem. Soc. Rev.*, 2013, **42**(8), 3318–3336.

5 Y. Taoda, T. Sawabe, Y. Endo, K. Yamaguchi, S. Fujii and H. Kagechika, Identification of an intermediate in the deboronation of *ortho*-carborane: An adduct of *ortho*-carborane with two nucleophiles on one boron atom, *Chem. Commun.*, 2008, **17**, 2049–2051.

6 L. I. Zakharkin and V. N. Kalinin, On the reaction of amines with barenes, *Tetrahedron Lett.*, 1965, **6**(7), 407–409.

7 R. A. Wiesboeck and M. F. Hawthorne, Dicarbaundecaborane(13) and Derivatives, *J. Am. Chem. Soc.*, 1964, **86**(8), 1642–1643.

8 M. G. Davidson, M. A. Fox, T. G. Hibbert, J. A. K. Howard, A. Mackinnon, I. S. Neretin and K. Wade, Deboronation of *ortho*-carborane by an iminophosphorane: Crystal structures of the novel carborane adduct *nido ortho* carborane tris(dimethylamino)iminophosphorane complex and the borenium salt $[(Me_2N)_3PNHBNP(NMe_2)_3]_2$-$O^{2+}(C_2B_9H_{12}^-)_2$, *Chem. Commun.*, 1999, (17), 1649–1650.

9 J. Yoo, J. W. Hwang and Y. Do, Facile and mild deboronation of *o*-carboranes using cesium fluoride, *Inorg. Chem.*, 2001, **40**(3), 568–570.

10 M. A. Fox and K. Wade, Cage-fluorination during deboronation of *meta*-carboranes, *Polyhedron*, 1997, **16**(14), 2517–2525.

11 M. A. Fox, J. A. H. MacBride and K. Wade, Fluoride-ion deboronation of *p*-fluorophenyl-*ortho*- and -*meta*-carboranes. NMR evidence for the new fluoroborate, HOBHF-2, *Polyhedron*, 1997, **16**(14), 2499–2507.

12 M. A. Fox, W. R. Gill, P. L. Herbertson, J. A. H. MacBride, K. Wade and H. M. Colquhoun, Deboronation of C-substituted *ortho*- and *meta-closo*-carboranes using "wet" fluoride ion solutions, *Polyhedron*, 1996, **15**(4), 565–571.

13 L. I. Zakharkin and V. S. Kirillova, *Izv. Akad. Nauk SSSR, Ser. Khim.*, 1975, 2596.

14 R. F. Barth, P. Mi and W. Yang, Boron delivery agents for neutron capture therapy of cancer, *Cancer Commun.*, 2018, **38**(1), 1–15.

15 *Boron-Based Compounds. Potential and Emerging applications in Medicine*, ed. E. Hey-Hawkins and C. Viñas Teixido, John Wiley & Sons Ltd, Chichester, UK, 2018.

16 *Boron Science, New Technologies and Applications*, ed. N. S. Hosmane, CRC Press, Boca Raton, FL, USA, 2012.

17 Boron, in *Medicine in Handbook of Boron Chemistry in Organometallics, Catalysis, Materials and Medicine*, ed. N. S. Hosmane and R. Eagling, World Science Publishers, New Jersey, 2018, vol. 4.

18 R. F. Barth, M. G. H. Vicente, O. K. Harling, W. S. Kiger, K. J. Riley, P. J. Binns, F. M. Wagner, M. Suzuki, T. Aihara, I. Kato and S. Kawabata, Current status of boron neutron capture therapy of high grade gliomas and recurrent head and neck cancer, *Radiat. Oncol.*, 2012, **7**(146), 1–21.

19 G. Calabrese, A. Daou, E. Barbu and J. Tsibouklis, Towards carborane-functionalised structures for the treatment of brain cancer, *Drug Discovery Today*, 2018, **23**(1), 63–75.

20 Z. Zheng, C. B. Knobler, M. D. Mortimer, G. Kong and M. Frederick Hawthorne, Hydrocarbon-Soluble Mercuracarborands: Syntheses, Halide Complexes, and Supramolecular Chemistry, *Inorg. Chem.*, 1996, **35**(5), 1235–1243.

21 E. L. Bregadze and L. P. Beletskaya, Synthesis of binuclear C-carboranylmercury and B-carboranylthallium complexes containing cyclopentadienyl and (dimethylaminomethylcyclopentadienyl)manganese tricarbonyl ligands, *Russ. Chem. Bull.*, 1993, **42**(3), 587–589.

22 J. Poater, M. Solà, C. Viñas and F. Teixidor, π Aromaticity and Three-Dimensional Aromaticity: Two sides of the Same Coin, *Angew. Chem., Int. Ed.*, 2014, **53**(45), 12191–12195.

23 G. M. A. Junqueira, Remarkable aromaticity of cobalt bis(dicarbollide) derivatives: a NICS study, *Theor. Chem. Acc.*, 2018, **137**(92), 1–7.

24 M. Couto, C. Alamón, C. Sánchez, B. Dávila, M. Fernández, N. Lecot, P. Cabral, F. Teixidor, C. Viñas and H. Cerecetto, Carboranylanilinoquinazoline stage in the drug-development pipeline, *Future Med. Chem.*, 2019, **11**(17), 2273–2285.

25 E. Oleshkevich, A. Morancho, A. Saha, K. M. O. Galenkamp, A. Grayston, S. G. Crich, D. Alberti, N. Protti, J. X. Comella, F. Teixidor, A. Rosell and C. Viñas, Combining magnetic nanoparticles and icosahedral boron clusters in biocompatible inorganic nanohybrids for cancer therapy, *Nanomedicine*, 2019, **20**(101986), 1–10.

26 I. Fuentes, T. García-Mendiola, S. Sato, M. Pita, H. Nakamura, E. Lorenzo, F. Teixidor, F. Marques and C. Viñas, Metallacarboranes on the Road to Anticancer Therapies: Cellular Uptake, DNA Interaction, and Biological Evaluation of Cobaltabisdicarbollide [COSAN]−, *Chem.–Eur. J.*, 2018, **24**(65), 17239–17254.

27 M. Couto, I. Mastandrea, M. Cabrera, P. Cabral, F. Teixidor, H. Cerecetto and C. Viñas, Small-Molecule Kinase-Inhibitors-Loaded Boron Cluster as Hybrid Agents for Glioma-Cell-Targeting Therapy, *Chem.–Eur. J.*, 2017, **23**(39), 9233–9238.

28 M. Couto, M. F. García, C. Alamón, M. Cabrera, P. Cabral, A. Merlino, F. Teixidor, H. Cerecetto and C. Viñas, Discovery of Potent EGFR Inhibitors through the Incorporation of a 3D-Aromatic-Boron-Rich-Cluster into the 4-Anilinoquinazoline Scaffold: Potential Drugs for Glioma Treatment, *Chem.–Eur. J.*, 2018, **24**(13), 3122–3126.

29 Z. J. Lesnikowski, Boron units as pharmacophores - New applications and opportunities of boron cluster chemistry, *Collect. Czech. Chem. Commun.*, 2007, **72**(12), 1646–1658.
30 S. Wang, C. Blaha, R. Santos, T. Huynh, T. R. Hayes, D. R. Beckford-Vera, J. E. Blecha, A. S. Hong, M. Fogarty, T. A. Hope, D. R. Raleigh, D. M. Wilson, M. J. Evans, H. F. Vanbrocklin, T. Ozawa and R. R. Flavell, Synthesis and Initial Biological Evaluation of Boron-Containing Prostate-Specific Membrane Antigen Ligands for Treatment of Prostate Cancer Using Boron Neutron Capture Therapy, *Mol. Pharm.*, 2019, **16**(9), 3831–3841.
31 S. Sato, S. Ishii and H. Nakamura, Development of Albumin-*closo*-Dodecaborate Conjugates as Boron Carriers for Neutron-Capture Therapy by Ru(bpy)3-Photocatalyzed Modification of Tyrosine, *Eur. J. Inorg. Chem.*, 2017, **2017**(38), 4406–4410.
32 T. He and R. A. Musah, Evaluation of the Potential of 2-Amino-3-(1,7-dicarba-*closo*-dodecaboranyl-1-thio)propanoic acid as a boron neutron capture therapy agent, *ACS Omega*, 2019, **4**(2), 3820–3826.
33 A. Isono, M. Tsuji, Y. Sanada, A. Matsushita, S. Masunaga, T. Hirayama and H. Nagasawa, Design, Synthesis, and Evaluation of Lipopeptide Conjugates of Mercaptoundecahydrododecaborate for Boron Neutron Capture Therapy, *ChemMedChem*, 2019, 823–832.
34 I. Nar, S. Bortolussi, I. Postuma, A. Atsay, E. Berksun, E. Viola, C. Ferrari, L. Cansolino, G. Ricciardi, M. P. Donzello and E. Hamuryudan, A Phthalocyanine-*ortho*-Carborane Conjugate for Boron Neutron Capture Therapy: Synthesis, Physicochemical Properties, and *in vitro* Tests, *ChemPlusChem*, 2019, **84**(4), 345–351.
35 A. N. Ay, H. Akar, A. Zaulet, C. Viñas, F. Teixidor and B. Zumreoglu-Karan, Carborane-layered double hydroxide nanohybrids for potential targeted- and magnetically targeted-BNCT applications, *Dalton Trans.*, 2017, **46**(10), 3303–3310.
36 D. Kaniowski, K. E. O. Nska, M. Sobczak, B. Wojtczak, S. Janczak, Z. J. Lésnikowski and B. Nawrot, High boron-loaded DNA-oligomers as potential boron neutron capture therapy and antisense oligonucleotide dual-action anticancer agents, *Molecules*, 2017, **22**(9), 1–20.
37 C. Viñas, R. Núñez, I. Bennour and F. Teixidor, Periphery Decorated and Core Initiated Neutral and Polyanionic Borane Large Molecules: Forthcoming and Promising Properties for Medicinal Applications, *Curr. Med. Chem.*, 2019, **26**(26), 5036–5076.
38 R. Frank, V. M. Ahrens, S. Boehnke, A. G. Beck-Sickinger and E. Hey-Hawkins, Charge-Compensated Metallacarborane Building Blocks for Conjugation with Peptides, *ChemBioChem*, 2016, **17**(4), 308–317.
39 Z. J. Lesnikowski, Nucleoside-boron cluster conjugates - Beyond pyrimidine nucleosides and carboranes, *J. Organomet. Chem.*, 2009, **694**(11), 1771–1775.
40 Z. J. Leśnikowski, E. Paradowska, A. B. Olejniczak, M. Studzińska, P. Seekamp, U. Schüßler, D. Gabel, R. F. Schinazi and J. Plešek, Towards new boron carriers for boron neutron capture therapy: Metallacarboranes and their nucleoside conjugates, *Bioorg. Med. Chem.*, 2005, **13**(13), 4168–4175.
41 M. Białek-Pietras, A. B. Olejniczak, S. Tachikawa, H. Nakamura and Z. J. Leśnikowski, Towards new boron carriers for boron neutron capture therapy: Metallacarboranes bearing cobalt, iron and chromium and their cholesterol conjugates, *Bioorg. Med. Chem.*, 2013, **21**(5), 1136–1142.
42 M. Gozzi, B. Schwarze, M. B. Sárosi, P. Lönnecke, D. Drača, D. Maksimović-Ivanić, S. Mijatović and E. Hey-Hawkins, Antiproliferative activity of (η^6-arene)ruthenacarborane sandwich complexes against HCT116 and MCF7 cell lines, *Dalton Trans.*, 2017, **46**(36), 12067–12080.
43 M. Gozzi, B. Schwarze and E. Hey-Hawkins, Half- and mixed-sandwich metallacarboranes for potential applications in medicine, *Pure Appl. Chem.*, 2019, **91**(4), 563–573.
44 N. P. E. Barry, A. Pitto-Barry, I. Romero-Canelón, J. Tran, J. J. Soldevila-Barreda, I. Hands-Portman, C. J. Smith, N. Kirby, A. P. Dove, R. K. O'Reilly and P. J. Sadler, Precious metal carborane polymer nanoparticles: Characterisation of micellar formulations and anticancer activity, *Faraday Discuss.*, 2014, **175**, 229–240.
45 I. Romero-Canelón, B. Phoenix, A. Pitto-Barry, J. Tran, J. J. Soldevila-Barreda, N. Kirby, S. Green, P. J. Sadler and N. P. E. Barry, Arene ruthenium dithiolato-carborane complexes for boron neutron capture therapy (BNCT), *J. Organomet. Chem.*, 2015, **796**, 17–25.
46 M. Gozzi, B. Murganic, D. Drača, J. Popp, P. Coburger, D. Maksimović-Ivanić, S. Mijatović and E. Hey-Hawkins, Quinoline-Conjugated Ruthenacarboranes: Towards Hybrid Drugs with Dual Mode of Action, *ChemMedChem*, 2019, **14**, 2061–2074.
47 L. Côrte-Real, M. Paula Robalo, F. Marques, G. Nogueira, F. Avecilla, T. J. L. Silva, F. C. Santos, A. Isabel Tomaz, M. Helena Garcia and A. Valente, The key role of coligands in novel ruthenium(II)-cyclopentadienyl bipyridine derivatives: Ranging from non-cytotoxic to highly cytotoxic compounds, *J. Inorg. Biochem.*, 2015, **150**, 148–159.
48 L. Côrte-Real, B. Karas, A. R. Brás, A. Pilon, F. Avecilla, F. Marques, A. Preto, B. T. Buckley, K. R. Cooper, C. Doherty, M. Helena Garcia and A. Valente, Ruthenium-Cyclopentadienyl Bipyridine-Biotin Based Compounds: Synthesis and Biological Effect, *Inorg. Chem.*, 2019, **58**(14), 9135–9149.
49 T. S. Morais, A. Valente, A. I. Tomaz, F. Marques and M. H. Garcia, Tracking antitumor metallodrugs: Promising agents with the Ru(II)- and Fe(II)-cyclopentadienyl scaffolds, *Future Med. Chem.*, 2016, **8**(5), 527–544.
50 L. Côrte-Real, F. Mendes, J. Coimbra, T. S. Morais, A. I. Tomaz, A. Valente, M. H. Garcia, I. Santos, M. Bicho and F. Marques, Anticancer activity of structurally related ruthenium(II) cyclopentadienyl complexes, *J. Biol. Inorg Chem.*, 2014, **19**(6), 853–867.
51 P. A. Jelliss, J. Mason, J. M. Nazzoli, J. H. Orlando, A. Vinson, N. P. Rath and M. J. Shaw, Synthesis and characterization of ruthenacarborane complexes incorporating chelating N-donor ligands: Unexpected luminescence from the

complex [3-CO-3,3-{κ^2-$Me_2N(CH_2)_2NMe_2$}-*closo*-3,1,2-$RuC_2B_9H_{11}$], *Inorg. Chem.*, 2006, **45**(1), 370–385.

52 O. Tutusaus, C. Viñas, R. Kivekäs, R. Sillanpää and F. Teixidor, Neutral *nido*-heteroboranes with non ionisable hydrogen as arenes in coordination, *Chem. Commun.*, 2003, 2458–2459.

53 O. Tutusaus, C. Viñas, R. Núñez, F. Teixidor, A. Demonceau, S. Delfosse, A. F. Noels, I. Mata and E. Molins, The modulating possibilities of dicarbollide clusters: Optimizing the Kharasch catalysts, *J. Am. Chem. Soc.*, 2003, **125**(39), 11830–11831.

54 O. Tutusaus, R. Núñez, C. Viñas, F. Teixidor, I. Mata and E. Molins, Synthesis, characterization, and dynamic studies of 12-vertex η^5-ruthenium(II) *closo*-phosphine complexes with monoanionic [10-L-*nido*-7-R-7,8-$C_2B_9H_9$] - ligands, *Inorg. Chem.*, 2004, **43**(19), 6067–6074.

55 R. Núñez, O. Tutusaus, F. Teixidor, C. Viñas, R. Sillanpää and R. Kivekäs, Formation of new η^5-rhodium(III) complexes from η^5-Rh(I) rhodacarborane-containing charge-compensated ligands, *Organometallics*, 2004, **23**(10), 2273–2280.

56 A. J. Welch, What can we learn from the crystal structures of metallacarboranes?, *Crystals*, 2017, **7**(8), 1–19.

57 K. J. Adams, J. Cowie, S. G. D. Henderson, G. J. McCormick and A. J. Welch, Steric effects in heteroboranes, *J. Organomet. Chem.*, 1994, **481**(2), C9–C11.

58 U. Gradler, A. S. Weller, A. J. Welch and D. Reedb, Synthesis, characterisation and molecular structures of the *closo* and *pseudocloso* heptamethylindenyl carbarhodaboranes 1-Ph=3-(eta-C_9Me_7)-3,1,2-*closo*-$RhC_2B_9H_{10}$ and 1,2-Ph_2-3-(eta-C_9Me_7)-3,1,2-*pseudocloso*-$RhC_2B_9H_9$. Experimental assignment of the ^{11}B NMR, *J. Chem. Soc., Dalton Trans.*, 1996, 335–342.

59 S. Hermanek, ^{11}B NMR Spectra of Boranes, Main-Group Heteroboranes, and Substituted Derivatives. Factors Influencing Chemical Shifts of Skeletal Atoms, *Chem. Rev.*, 1992, **92**(2), 325–362.

60 R. J. Wilson, L. F. Warren and M. F. Hawthorne, The Existence of the Nickel(IV) Dication Derived from Nickelocene and a Cationic Boron Hydride Analog, *J. Am. Chem. Soc.*, 1969, **91**(3), 758–759.

61 S. Chardon-noblat, A. Deronzier, D. Zsoldos, R. Ziessel, M. Haukka, T. Pakkanen and T. Venalainen, Mode of formation of polymeric [{Ru(bipy)$(CO)_2$}$_n$] (bipy = 2,2′-bipyridine) films, *J. Chem. Soc., Dalton Trans.*, 1996, 2582–2583.

62 L. Pauling, *The Nature of the Chemical Bond*, Cornell University Press, Ithaca, NY, 3rd edn, 1960.

63 R. F. Barth, Z. Zhang and T. Liu, A realistic appraisal of boron neutron capture therapy as a cancer treatment modality, *Cancer Commun.*, 2018, **38**(36), 1–7.

64 R. F. Barth, J. A. Coderre, M. G. H. Vicente and T. E. Blue, Boron neutron capture therapy of cancer: Current status and future prospects, *Clin. Cancer Res.*, 2005, **11**(11), 3987–4002.

65 R. F. Barth, Boron neutron capture therapy at the crossroads: Challenges and opportunities, *Appl. Radiat. Isot.*, 2009, **67**(7–8 suppl.), 67–70.

66 S. Anderson, D. F. Mullica, E. L. Sappenfield and F. G. A. Stone, Carborane Complexes of Ruthenium: A Convenient Synthesis of [$Ru(CO)_3$(η^5-7,8-$C_2B_9H_{11}$)] and a Study of Reactions of This Complex, *Organometallics*, 1995, **14**(7), 3516–3526.

67 A. McAnaw, G. Scott, L. Elrick, G. M. Rosair and A. J. Welch, The VCD method - A simple and reliable way to distinguish cage C and B atoms in (hetero)carborane structures determined crystallographically, *Dalton Trans.*, 2013, **42**(3), 645–664.

68 J. Catterick, M. B. Hursthouse, P. Thornton and A. J. Welch, Crystal and Molecular Structure of Tetra-*p*-benzoato-bisquinolinedi- cobalt(II), a Binuclear Cobalt(II) Carboxylate, *J. Chem. Soc., Dalton Trans.*, 1977, 223–226.

69 A. L. Spek, Structure validation in chemical crystallography, *Acta Crystallogr., Sect. D: Biol. Crystallogr.*, 2009, **65**(2), 148–155.

70 Bruker Advanced X-ray Solutions, *SMART: Version 5.631*.

71 Bruker Advanced X-ray Solutions, *SAINT+, Version 6.36A*, 2001.

72 G. M. Sheldrick, *Empirical Absorption Correction Program*, Universität Göttingen, 1996.

73 Bruker Advanced X-ray Solutions, *SADABS Version 2.10*, 2001.

74 G. M. Sheldrick, *Program for Crystal Structure Refinement*, Universität Göttingen, 1997.

75 G. M. Sheldrick, *SHELXT-SHELXL-2014/7*, 2014.

76 L. Côrte-Real, A. P. Matos, I. Alho, T. S. Morais, A. I. Tomaz, M. H. Garcia, I. Santos, M. P. Bicho and F. Marques, Cellular uptake mechanisms of an antitumor ruthenium compound: The endosomal/lysosomal system as a target for anticancer metal-based drugs, *Microsc. Microanal.*, 2013, **19**(5), 1122–1130.

